

Theoretical study on the kesterite solar cells based on $Cu_2ZnSn(S,Se)_4$ and related photovoltaic semiconductors

Dingrong Liu(刘定荣), Dan Han(韩丹), Menglin Huang(黄梦麟), Xian Zhang(张弦), Tao Zhang(张涛), Chenmin Dai(戴称民), Shiyou Chen(陈时友)
Citation: Chin. Phys. B . 2018, 27(1): 018806. **doi:** 10.1088/1674-1056/27/1/018806

Journal homepage: http://cpb.iphy.ac.cn; http://iopscience.iop.org/cpb

What follows is a list of articles you may be interested in

Electronic structure and optical properties of Al and Mg co-doped GaN

Ji Yan-Jun, Du Yu-Jie, Wang Mei-Shan
Chin. Phys. B . 2013, 22(11): 117103. **doi:** 10.1088/1674-1056/22/11/117103

First-principles calculations of electronic and magnetic properties of CeN：The LDA+*U* method

Hao Ai-Min, Bai Jing
Chin. Phys. B . 2013, 22(10): 107102. **doi:** 10.1088/1674-1056/22/10/107102

First-principles study on nonlocal ferromagnetism in (Cu, N)-codoped ZnO

Qin Guo-Ping, Wang Xin-Qiang, Zheng Ji, Kong Chun-Yang, Ruan Hai-Bo, Li Wan-Jun, Zhao Yong-Hong, Meng Xiang-Dan
Chin. Phys. B . 2013, 22(5): 057101. **doi:** 10.1088/1674-1056/22/5/057101

Phase transition and thermodynamic properties of $BiFeO_3$ from first-principles calculations

Li Qiang, Huang Duo-Hui, Cao Qi-Long, Wang Fan-Hou
Chin. Phys. B . 2013, 22(3): 037101. **doi:** 10.1088/1674-1056/22/3/037101

Multiscale simulations in face-centered cubic metals: A method coupling quantum mechanics and molecular mechanics

Yu Xiao-Xiang, Wang Chong-Yu
Chin. Phys. B . 2013, 22(2): 027101. **doi:** 10.1088/1674-1056/22/2/027101

TOPICAL REVIEW — New generation solar cells

Theoretical study on the kesterite solar cells based on $Cu_2ZnSn(S,Se)_4$ and related photovoltaic semiconductors*

Dingrong Liu(刘定荣)[1,†], Dan Han(韩丹)[1,†], Menglin Huang(黄梦麟)[1,†], Xian Zhang(张弦)[1], Tao Zhang(张涛)[1], Chenmin Dai(戴称民)[1], and Shiyou Chen (陈时友)[1,2,‡]

[1] *Key Laboratory of Polar Materials and Devices (MOE), East China Normal University, Shanghai* 200241, *China*
[2] *Collaborative Innovation Center of Extreme Optics, Shanxi University, Taiyuan* 030006, *China*

(Received 16 October 2017; revised manuscript received 17 November 2017; published online 13 December 2017)

The kesterite thin film solar cells based on the quaternary Cu_2ZnSnS_4 and $Cu_2ZnSnSe_4$ and their alloys $Cu_2ZnSn(S,Se)_4$ have been considered as environment-friendly and non-toxic alternatives to the currently commercialized CdTe and $Cu(In,Ga)Se_2$ thin film solar cells. From the theoretical point of view, we will review how the group I_2–II–IV–VI_4 quaternary compound semiconductors are derived from the binary CdTe and the ternary $CuInSe_2$ or $CuGaSe_2$ through the cation mutation, and how the crystal structure and electronic band structure evolve as the component elements change. The increased structural and chemical freedom in these quaternary semiconductors opens up new possibility for the tailoring of material properties and design of new light-absorber semiconductors. However, the increased freedom also makes the development of high-efficiency solar cells more challenging because much more intrinsic point defects, secondary phases, surfaces, and grain-boundaries can exist in the thin films and influence the photovoltaic performance in a way different from that in the conventional CdTe and $Cu(In,Ga)Se_2$ solar cells. The experimental characterization of the properties of defects, secondary phase, and grain-boundaries is currently not very efficient and direct, especially for these quaternary compounds. First-principles calculations have been successfully used in the past decade for studying these properties. Here we will review the theoretical progress in the study of the mixed-cation and mixed-anion alloys of the group I_2–II–IV–VI_4 semiconductors, defects, alkaline dopants, and grain boundaries, which provided very important information for the optimization of the kesterite solar cell performance.

Keywords: kesterite thin film solar cells, Cu_2ZnSnS_4 and $Cu_2ZnSnSe_4$, first-principles calculations, defects and dopants

PACS: 88.40.H–, 71.20.Nr, 61.50.Ah, 71.20.–b **DOI:** 10.1088/1674-1056/27/1/018806

1. Introduction

The kesterite semiconductors Cu_2ZnSnS_4 and $Cu_2ZnSnSe_4$ and their alloys $Cu_2ZnSn(S,Se)_4$ have drawn intensive attention as the light-absorber materials in thin film solar cells since 2010.[1–3] The rapid development of the kesterite solar cells in the past years has been reviewed in a series of review papers or books[4] as well as in this special issue.

Both Cu_2ZnSnS_4 and $Cu_2ZnSnSe_4$ belong to the group I_2–II–IV–VI_4 quaternary compound semiconductors. The study on the I_2–II–IV–VI_4 quaternary semiconductors dates back to 1950s, and a series of I_2–II–IV–VI_4 semiconductors have been synthesized by different methods.[5–8] From the view of theoretical material design, the quaternary I_2–II–IV–VI_4 semiconductors, in which both the anions and cations have tetrahedral coordination, can be designed through a two-step cation mutation (substitution) from the binary II–VI semiconductors in the zincblende or wurtzite structure with tetrahedral coordination,[1,9–13] as shown schematically in Fig. 1. For example, the zincblende-structured ZnSe mutates into the chalcopyrite-structured $CuGaSe_2$ through replacing two Zn by one Cu and one Ga, and the chalcopyrite-structured $CuGaSe_2$ further mutates into the kesterite-structured $Cu_2ZnSnSe_4$ through replacing two Ga by one Zn and one Sn, giving the mutation from binary compound semiconductors to the quaternary compound semiconductors, ZnSe→$CuGaSe_2$ →$Cu_2ZnSnSe_4$. By choosing different component elements, a series of I_2–II–IV–VI_4 quaternary compounds can be derived, as shown in Fig. 1. The mutation derivation of new ternary and quaternary compound semiconductors is possible not only from the II–VI semiconductors such as ZnSe, but also from the III–V semiconductors such as GaN and GaP, with a series of new nitrides and phosphides designed recently.[11,14,15]

The application of Cu_2ZnSnS_4 (CZTS) in solar cells dates back to 1988 when Ito and Nakazawa synthesized Cu_2CdSnS_4 and Cu_2ZnSnS_4 thin films, fabricated a CZTS solar cell, and reported a 165 meV open-circuit voltage.[16] During the 14 years from 1996 to 2009, Katagiri *et al.* have pioneered the fabrication of Cu_2ZnSnS_4 thin film solar cells with a

*Project supported by the National Key Research and Development Program of China (Grant No. 2016YFB0700700), the National Natural Science Foundation of China (Grant Nos. 61574059 and 61722402), Shu-Guang Program, China (Grant No. 15SG20), and CC of ECNU, China.

†There authors contributed equally to this work.

‡Corresponding author. E-mail: chensy@ee.ecnu.edu.cn

© 2018 Chinese Physical Society and IOP Publishing Ltd

device structure ZnO:Al/CdS/CZTS/Mo/SLG (similar to that of the Cu(In,Ga)Se_2 solar cells), and increased the energy-conversion efficiency from 0.66% (an open-circuit voltage of 400 mV) in 1996 to 6.7% in 2009.[3,17] In 1997, Friedlmeier *et al.* also fabricated a Cu_2ZnSnS_4 solar cell with 2.3% efficiency and a $Cu_2ZnSnSe_4$ cell with 0.6% efficiency.[18]

Despite the steady efficiency increase during the period of 1996–2009, Cu_2ZnSnS_4, $Cu_2ZnSnSe_4$, and also all other I_2–II–IV–VI_4 semiconductors had not attracted special attention in the photovoltaic field, and many fundamental properties (crystal structure, electronic structure, optical properties) of I_2–II–IV–VI_4 had not been well characterized and were even wrong.[19] Until 2009, $Cu_2ZnSnSe_4$ was even reported experimentally to crystallize in the stannite structure (rather than the kesterite structure), and its band gap was reported to be around 1.5 eV, which is close to that of Cu_2ZnSnS_4, indicating that it is impossible to tune the band gap through forming $Cu_2ZnSn(S,Se)_4$ alloys.[1,9] Using the first-principles calculations, we studied the chemical trends in the crystal structure and electronic band structure of a series of I_2–II–IV–VI_4 semiconductors, showing that the ground-state structure of $Cu_2ZnSnSe_4$ is the kesterite structure and its band gap is 1.0 eV (0.5 eV smaller than that of Cu_2ZnSnS_4), and thus pointed out the long-standing misunderstanding in the crystal structure[20] and band gaps of $Cu_2ZnSnSe_4$ as well as other I_2–II–IV–VI_4 semiconductors.[1,9]

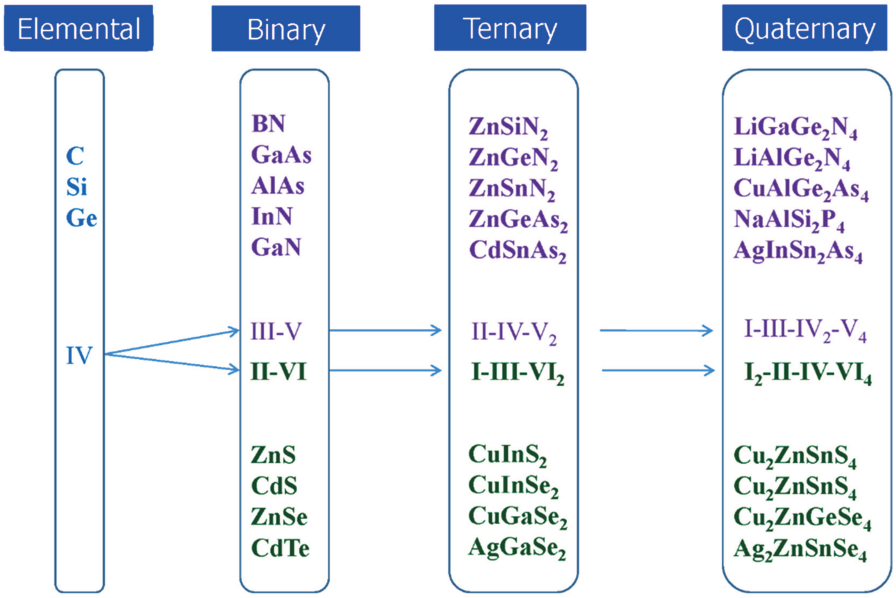


Fig. 1. (color online) The schematic plot of the cation-mutation from the group IV elemental semiconductors to the group III–V and II–VI binary compound semiconductors, and then to the group II–IV–V_2 and I–III–VI_2 ternary compound semiconductors and the group I–III-IV_2–V_4 and I_2–II–IV–VI_4 quaternary compound semiconductors.[1,9–13]

Since 2010, the Cu_2ZnSnS_4 and $Cu_2ZnSnSe_4$ systems become a hot topic in the photovoltaic field, especially after the publication of the experimental paper by Mitzi *et al.* who reported a hydrazine-based deposition of the $Cu_2ZnSn(S,Se)_4$ (CZTSSe) alloys and a fabrication of a 9.7% efficiency solar cell based on the CZTSSe alloys.[2] The record efficiency was then increased to 11.1% in 2012,[21] and to 12.6% in 2013.[22] In 2010, Ahn *et al.* also reported their experimental determination of the band gap of $Cu_2ZnSnSe_4$ at 1.02 eV.[23] Nowadays the thin film solar cells using Cu_2ZnSnS_4 (with a band gap at 1.5 eV), $Cu_2ZnSnSe_4$ (with a band gap at 1.0 eV), and their alloys $Cu_2ZnSn(S,Se)_4$ (with a linearly and continuously tunable band gap from 1.0 eV to 1.5 eV) as the light-absorber layer are called CZTS, CZTSe, and CZTSSe solar cells, respectively, or more generally kesterite solar cells.

The fundamental crystal structure, electronic structure, and defect properties have been reviewed in a series of papers[13,24,25] or book chapters.[4] Here we will introduce the crystal structure and electronic band structure first, and review the theoretical study on the mixed-cation and mixed-anion alloys, alkaline dopants, and grain boundaries in detail, which we believe will be very important for the further optimization of the kesterite solar cell performance.

2. Crystal structure

Since the I_2–II–IV–VI_4 semiconductors can be derived from the binary II–VI semiconductors which usually crystallize in the zincblende or wurtzite structure with the tetrahedral coordination, their crystal structures can also be derived from the zincblende and wurtzite structures, as shown in Fig. 2. By following the electronic octet rule (the eight-electron full-shell state has lower energy), two ternary structures (chalcopyrite and CuAu structures) can be derived from the zincblende structure, and then the quaternary kesterite structure can be derived from the chalcopyrite structure, while the stannite structure and primitive-mixed CuAu structure can be derived from the CuAu structure.[1,9] Total energy calculations showed

clearly that the kesterite structure has lower energy than the other structures for Cu_2ZnSnS_4, $Cu_2ZnSnSe_4$, Cu_2ZnGeS_4, and other I_2–II–IV–VI_4 semiconductors with small cation-size difference,[1,9] which can be understood according to the lower Coulomb energy (Madelung energy) and strain energy of the kesterite structure than the other structures.[26,27]

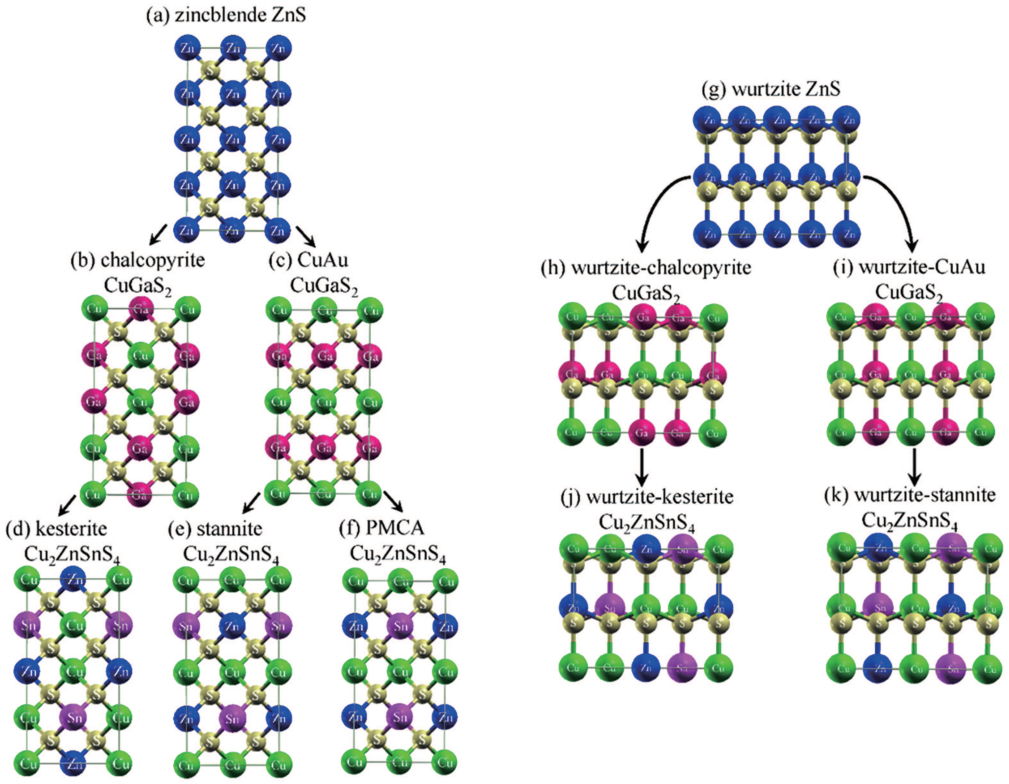


Fig. 2. (color online) The crystal structure mutation from (a) zinc-blende ZnS to (b) chalcopyrite $CuGaS_2$ and (c) CuAu-like $CuGaS_2$, then to (d) kesterite Cu_2ZnSnS_4, (e) stannite Cu_2ZnSnS_4, and (f) PMCA-Cu_2ZnSnS_4, and the mutation from (g) wurtzite ZnS to (h) wurtzite-chalcopyrite $CuGaS_2$ and (i) wurtzite-CuAu $CuGaS_2$, then to (j) wurtzite-kesterite Cu_2ZnSnS_4 and (k) wurtzite-stannite Cu_2ZnSnS_4. Adapted from Refs. [4], [9], and [10].

However, when the cation-size difference is large, both the kesterite and stannite structures may become the lowest-energy structures, e.g., the stannite structure has lower energy than kesterite for Cu_2Cd–IV–S_4, while Ag_2ZnSnS_4 and $Ag_2ZnSnSe_4$ are still more stable in the kesterite structure. Zhang *et al.*[28] have studied a series of Cu-based quaternary semiconductors and proposed that the stannite structure is energetically more stable for systems containing Cd. The calculated lowest-energy structures for a series of I_2–II–IV–VI_4 semiconductors can be found in Ref. [20]. For the lattice constants, no matter the ground state structure is kesterite or stannite, the most stable one always has larger a and smaller $\eta = c/2a$.[9,28]

The crystal structure mutation is also possible for the wurtzite structure. As shown in Figs. 2(g)–2(k), two wurtzite-derived ternary structures (we name them the wurtzite-chalcopyrite and wurtzite-CuAu structures) and two wurtzite-derived quaternary structures (we name them the wurtzite-kesterite and wurtzite-stannite structures) can be derived from the binary wurtzite structure. These wurtzite-derived structures can be corresponding to the zincblende-derived structures, as shown by their names, i.e., when the kesterite structure is more stable than the stannite structure, the wurtzite-kesterite structure is more stable than the wurtzite-stannite structure. Usually the quaternary I_2–II–IV–VI_4 semiconductors with small and very ionic elements tend to have wurtzite-kesterite or wurtzite-stannite as their ground-state structures, e.g., Cu_2CdSiS_4 and $Cu_2CdSiSe_4$ are more stable in the wurtzite-stannite structure, while Cu_2ZnSiS_4 and $Cu_2ZnSiSe_4$ are more stable in the kesterite structure. Nakamura *et al.*[29] also showed that $Cu_2ZnSiSe_4$ is more stable in the kesterite structure, which is consistent with our calculation. However, since the energy difference between the wurtzite-derived and zincblende-derived structures is very small for some I_2–II–IV–VI_4 semiconductors, the real structure of the samples may be sensitive to synthesis kinetics.

Although the ground state structures of Cu_2ZnSnS_4, $Cu_2ZnSnSe_4$, Cu_2ZnGeS_4, and other I_2–II–IV–VI_4 semiconductors have been determined, the unique partial disorder makes the real structure of the synthesized thin films more complicated for the standard x-ray diffraction characterization. In kesterite structure, the /Cu+Zn/Cu+Sn/Zn+Cu/Sn+Cu/ layers are ordered along the (001) direction, as shown in Fig. 3(a), and all the anions satisfy the electronic octet rule. The occupation of Zn and Cu cations in

the third layer can be exchanged, changing the order to /Cu+Zn/Cu+Sn/Cu+Zn/Sn+Cu/, which does not violate the octet rule, and the calculated energy of this new structure is slightly higher (by less than 1 meV/atom) than that of the kesterite, and lower than that of the stannite (which is 3 meV/atom higher than that of the kesterite). Since the energy cost for the exchange of Cu and Zn cations in the (001) layers is very small, the Cu and Zn sites in the (001) layers become partially disordered at the growth temperature (which is usually much higher than room temperature), as shown in Fig. 3(b). With the partial disorder in the Cu+Zn (001) layer (disordered Cu and Zn can be considered as one element), the kesterite structure has the same symmetry as the stannite structure. The atomic numbers (form factors) of Cu and Zn are similar, so the partially disordered kesterite structure and the stannite structure cannot be distinguished using the standard x-ray diffraction measurements, explaining why $Cu_2ZnSnSe_4$ and $Cu_2ZnGeSe_4$ used to be reported to crystallize in the stannite structure in many experimental papers before 2009. The recent neutron scattering measurements by Schorr *et al.* and synchrotron radiation x-ray diffraction measurements by Washio *et al.* both observed the existence of the Cu + Zn partial disorder in Cu_2ZnSnS_4 and $Cu_2ZnSnSe_4$.[20,30,31]

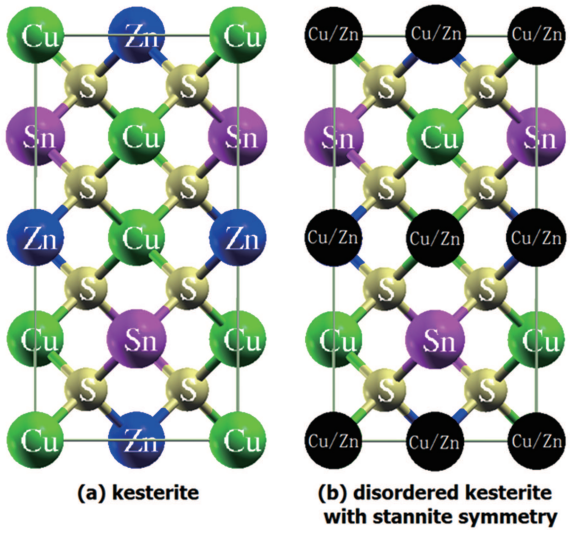


Fig. 3. (color online) The crystal structures of (a) the kesterite and (b) Cu/Zn partially disordered kesterite Cu_2ZnSnS_4. Partially disordered means that the Cu/Zn disordered occupation exists only in the (001) CuZn layers, so the symmetry of the crystal lattice is also *I*-4, equivalent to that of the stannite structure. Adapted from Ref. [4].

It is also interesting to see that the partial disorder in the (001) layers has negligible influence on the electronic structure, so its influence on the electrical properties may be small although the partial disorder may increase the carrier scattering and decrease the mobility. In contrast, the structure change from kesterite to stannite can decrease the band gap by 0.2 eV. The exchange of Cu and Zn in the kesterite structure (formation of a Cu_{Zn}+Zn_{Cu} antisite pair in a 128-atom supercell) decreases the band gap by about 0.1 eV and costs a formation energy about 0.2 eV/pair. As we can see, the partial disorder in the (001) layer costs less energy and also induces smaller band gap change than single antisite-pair or the structure change from kesterite to stannite.

Since 2013, the cation mutation has attracted more attention, and Be, Mg, Ca, Sr, and Ba are also considered as the group II cations, whereas Ti, Zr, and Hf are considered as the group IV cations.[32–36] One important reason for the substitution of elements is to increase the size difference between the cations and thus suppress the formation of caton antisites. Zhong *et al.*[33] showed in 2016 that when Zn is replaced by Mg and Ca, leading to Cu_2MgSnS_4 and Cu_2CaSnS_4, respectively, the lowest-energy (ground state) structure changes from kesterite to stannite, which shows the same trend as in the case of Cu_2Cd–IV–S_4 series. In 2017, Chen *et al.*[36] calculated the electronic structure of Cu_2BeSnS_4 and predicted a band gap of 1.76 eV, and also showed that Cu_2BeSnS_4 exhibits benign defect properties for the large difference of its atomic size, thus evidently lowering the concentration of the antisite defects. The absorption coefficient is as high as 10^5 cm^{-1} according to their calculation. However, the toxic element Be limits the development of practical solar cells.

Interestingly, Cu_2–II–Sn–VI_4 (II = Ba, Sr; VI = S, Se) were proposed as promising light-absorber materials for solar cells and photoelectrochemical water-splitting applications during the last year.[34,35] For these systems with very large group II cations, the crystal structure is very different from the kesterite or stannite structure, and the lowest-energy structure is usually not those with the tetrahedral coordination. Since the commercialized solar cells are most based on Si, CdTe, and Cu(In,Ga)Se_2 with tetrahedral coordination, it will be interesting to see the photovoltaic semiconductors with non-tetrahedral coordination, such as the perovskite semiconductors.

3. Electronic band structure

The electronic structure analysis is helpful for understanding the electrical conductivity of the I_2–II–IV–VI_4 semiconductors and why the band gaps and band edge positions change as the component elements change. The chemical trends in the band gaps of these semiconductors have been summarized in Ref. [37]. Figure 4 shows the calculated band structure, density of states, and band component analysis for the kesterite Cu_2ZnSnS_4. We can see: (i) Cu_2ZnSnS_4 is a direct bandgap semiconductor, (ii) the valence band maximum (VBM) state depends on the orbital hybridization between Cu 3d (t_{2g}) and S 3p, and the conduction band minimum (CBM) state is composed mainly of Sn 5s and S 3s, 3p, and (iii) the group II cation Zn has little contribution to the band gap (va-

lence and conduction band edges).[38–41] Similar characteristics exist for the band structure of $Cu_2ZnSnSe_4$, despite that the band gap is smaller by 0.5 eV and the valence band dispersion is larger than that of Cu_2ZnSnS_4.

Compared to ZnS, the Cu-based chalcogenides, such as Cu_2ZnGeS_4, have much smaller band gaps, because the valence band edge is much higher due to the shallower Cu 3d levels, which can be seen clearly in the calculated band alignment in Fig. 5(a). The valence band edge of $CuGaS_2$ and Cu_2ZnGeS_4 is about 1.15 eV higher that of ZnS. The band gap of Cu_2ZnGeS_4 is also smaller than that of $CuGaS_2$ because the conduction band edge is lower due to the lower Ge 4s level than the Ga 4s orbital.

Similarly, the valence band edge of Cu_2ZnSnS_4 is about 1 eV higher than that of Cu-free CdS, as shown in Fig. 5(b). Since the band gap of CdS is 2.42 eV and that of Cu_2ZnSnS_4 is 1.5 eV, the conduction band edge of Cu_2ZnSnS_4 is about 0.1 eV higher than that of CdS, giving a type-II band alignment between Cu_2ZnSnS_4 and CdS. The valence band edge of $Cu_2ZnSnSe_4$ is 0.15 eV higher than that of Cu_2ZnSnS_4, while its conduction band edge is 0.35 eV lower than that of Cu_2ZnSnS_4. As we know, the VBM of quaternary Cu_2ZnSnS_4 and $Cu_2ZnSnSe_4$ is an antibonding state of the hybridization between Cu d orbitals and anion p orbitals.[9] It is well known that the Se p level is higher than S p level, but due to that the shorter Cu–S bond makes the p–d hybridization stronger, the valence band offset between Cu_2ZnSnS_4 and $Cu_2ZnSnSe_4$ is just 0.15 eV. On the other hand, the anion s and Sn s orbitals compose the CBM and the shorter Sn–S bond makes the s–s level repulsion stronger, thus moving the CBM of the Cu_2ZnSnS_4 higher than that of $Cu_2ZnSnSe_4$. It is obvious that the CBM downshift plays a more important role for the bandgap reduction from Cu_2ZnSnS_4 to $Cu_2ZnSnSe_4$.

The conduction band edge of $Cu_2ZnSnSe_4$ is 0.25 eV lower than that of CdS, giving a type-I band alignment between $Cu_2ZnSnSe_4$ and CdS. The type-I and type-II band alignment difference of Cu_2ZnSnS_4 and $Cu_2ZnSnSe_4$ relative to CdS has been discussed in Ref. [42]. The experimental measurement of the valence band offset between $Cu_2ZnSnSe_4$ and CdS is around 0.9–1.2 eV.[42–48] The 0.3 eV difference may result from the different interfaces, elemental composition ratios, and measurement methods used by different groups. If the valence band offset is only 0.9 eV, the band alignment between Cu_2ZnSnS_4 and CdS becomes type-I. The accurate measurement of the band offset and the influence of the different interfaces, elemental composition ratios, and measurement methods on the results are still interesting topics deserving further study.

Different structures (kesterite, stannite, and PMCA) have the valence band edges close to each other, while the conduction band edge shifts down from kesterite to stannite and PMCA, leading to smaller band gaps of stannite and PMCA. Figure 6 shows the calculated band gaps of Cu_2ZnSiS_4, Cu_2ZnGeS_4, and Cu_2ZnSnS_4, which shows clearly that the kesterite structure always has larger band gap than the stannite structure, and the wurtzite-derived structure always has larger band gap than the corresponding zincblende-derived structure.[9,10] The larger band gap of the wurtzite structure than the zincblende structure has also been noticed in binary II–VI semiconductors.[19]

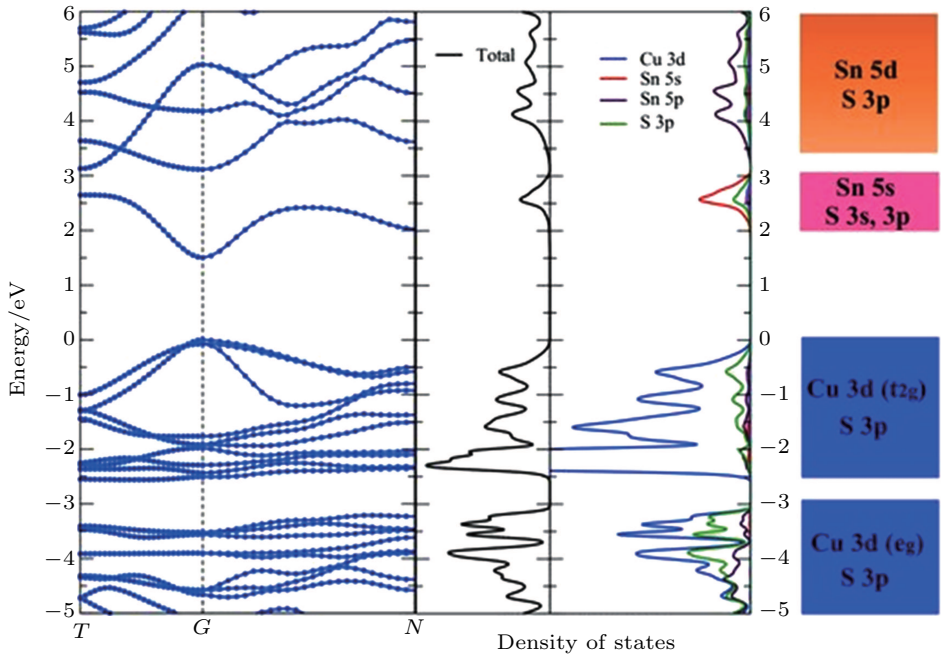


Fig. 4. (color online) The calculated band structure, total and partial density of states, and the schematic plot of the band component for kesterite Cu_2ZnSnS_4. Adapted from Ref. [24].

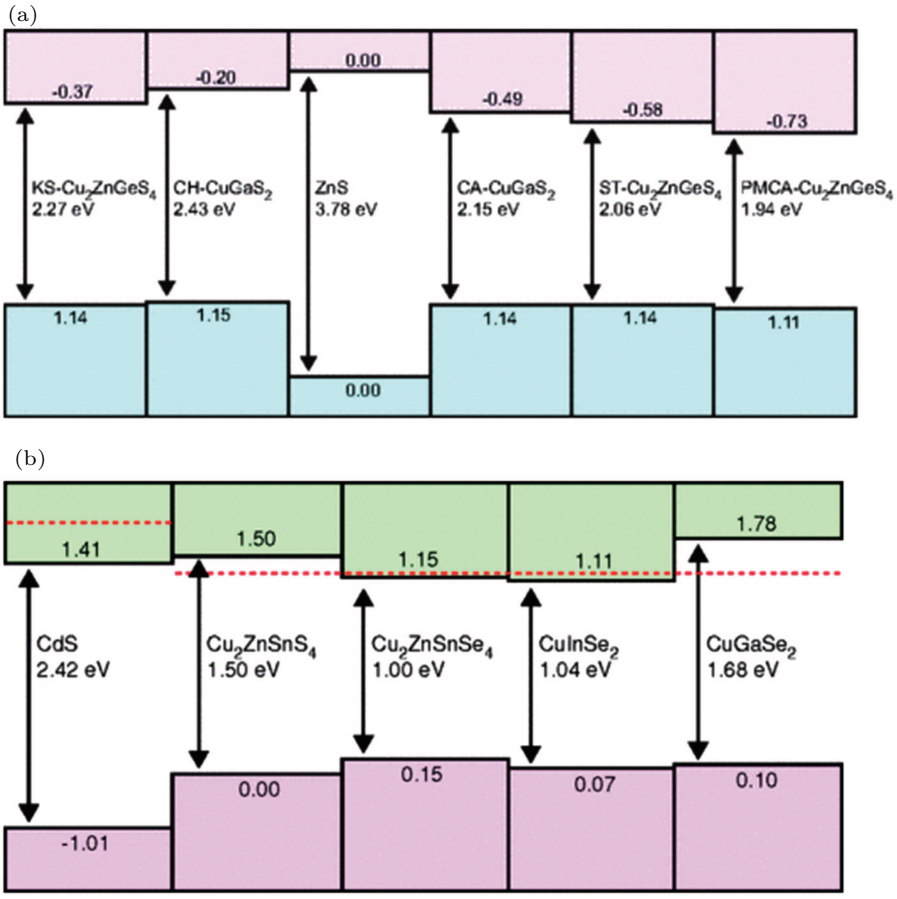


Fig. 5. (color online) (a) The calculated band alignment of ZnS, $CuGaS_2$, and Cu_2ZnGeS_4. Adapted from Ref. [9]. (b) The calculated band alignment of binary CdS, ternary $CuInSe_2$ and $CuGaSe_2$, and quaternary Cu_2ZnSnS_4 and $Cu_2ZnSnSe_4$. The red dashed lines near the conduction band show the n-type doping limit. Adapted from Ref. [42].

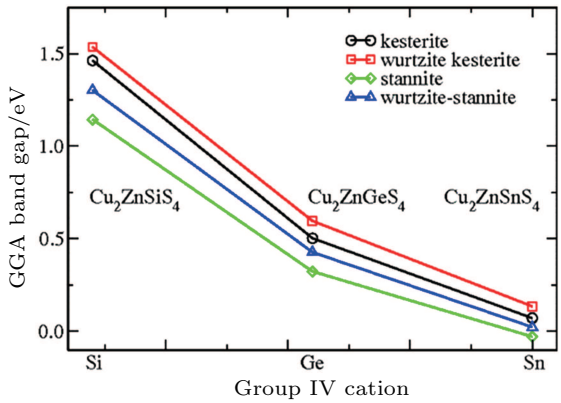


Fig. 6. (color online) The GGA calculated band gaps of CuZn–IV–S_4. Compared to the experimental values, the GGA calculated values have a general underestimation by about 1.4 eV for these semiconductors. Adapted from Ref. [10].

Liu *et al.*[49] have studied the electron and hole effective masses of KS and ST structured Cu_2Zn–IV–VI_4. They found that the electron effective masses are rather small and almost isotropic while the hole effective masses show strong anisotropies, and the effective masses of the Se-based compounds are much smaller than those of the S-based compounds. Table 1 shows the electron and hole effective masses calculated from band energy dispersions. For the conduction band, both longitudinal and transverse electron effective masses are rather small and similar. For the valence band, the longitudinal and transverse hole effective masses are calculated from the topmost 3 valence bands. Interestingly, the trend is apparent for all of the chosen quaternary compounds: for the kesterite structure, the 1st VB has a much smaller hole effective mass along the *c*-axis (longitudinal masses) than the other two VBs. However, the stannite structure has an opposite ordering in the band, which shows that the 3rd VB has the smaller effective mass than the topmost 2 VBs.

The different hole effective masses for the kesterite and stannite structures result from the opposite crystal filed splitting,[9,50] and can be understood by their partial charge densities shown in Fig. 7. For the kesterite structure, the p orbitals in sulfur of the 1st VB are parallel to the *c*-axis, which is the same to those of the 3rd VB in the stannite structure. The remaining two VBs both in kesterite and stannite structures also have the same p orbital configurations.

Table 1. The Γ point electron effective masses (m_c) and hole effective masses (m_n for n = v1, v2, and v3, where v1 is the topmost valence band) calculated from the band-energy dispersions. The longitudinal masses $m^{\parallel}$ are determined from the dispersions along the (001) direction, while the transverse masses $m^{\perp}$ are derived from the dispersions in both the (110) and (100) directions. The values are in unit of the free electron mass m_e. Adapted from Ref. [49].

	Cu_2ZnSnS_4		Cu_2ZnGeS_4		Cu_2ZnSiS_4	
	Kesterite	Stannite	Kesterite	Stannite	Kesterite	Stannite
$m^{\parallel}_{c1}$	0.18	0.18	0.21	0.22	0.26	0.29
$m^{\perp}_{c1}$	0.19	0.19	0.22	0.21	0.24	0.22
$m^{\parallel}_{v1}$	0.22	0.74	0.27	0.67	0.4	0.71
$m^{\perp}_{v1}$	0.74	0.34	0.91	0.41	2.45	0.55
$m^{\parallel}_{v2}$	0.65	0.69	0.65	0.63	0.67	0.66
$m^{\perp}_{v2}$	0.34	0.32	0.37	0.38	0.47	0.52
$m^{\parallel}_{v3}$	0.66	0.2	0.63	0.25	0.67	0.38
$m^{\perp}_{v3}$	0.3	0.69	0.34	0.83	0.44	1.52
	$Cu_2ZnSnSe_4$		$Cu_2ZnGeSe_4$		$Cu_2ZnSiSe_4$	
	Kesterite	Stannite	Kesterite	Stannite	Kesterite	Stannite
$m^{\parallel}_{c1}$	0.1	0.09	0.11	0.11	0.15	0.16
$m^{\perp}_{c1}$	0.11	0.1	0.12	0.11	0.15	0.14
$m^{\parallel}_{v1}$	0.12	0.55	0.13	0.5	0.21	0.52
$m^{\perp}_{v1}$	0.32	0.14	0.38	0.17	0.58	0.27
$m^{\parallel}_{v2}$	0.53	0.13	0.51	0.2	0.54	0.39
$m^{\perp}_{v2}$	0.16	0.23	0.18	0.23	0.26	0.32
$m^{\parallel}_{v3}$	0.34	0.18	0.39	0.16	0.47	0.21
$m^{\perp}_{v3}$	0.26	0.35	0.29	0.48	0.39	0.81

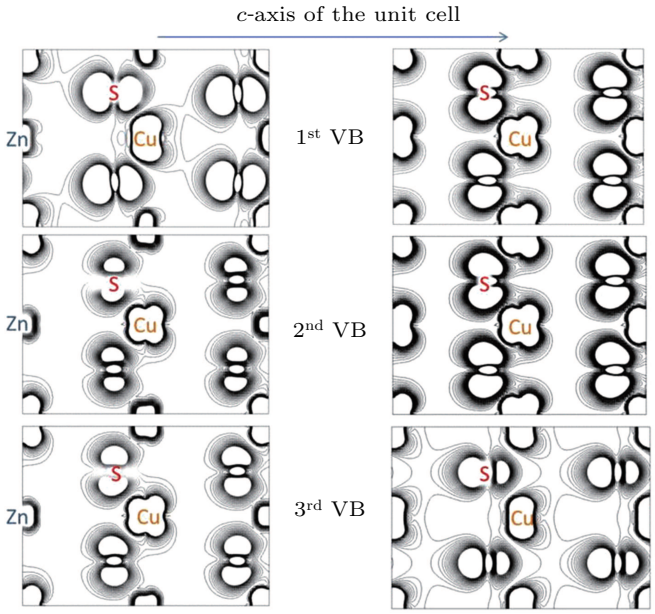


Fig. 7. (color online) Partial charge density of the topmost 3 VBs at the Γ point in (a) the Cu–S–Zn plane for the kesterite Cu_2ZnGeS_4 and (b) the Cu–S plane for the stannite Cu_2ZnGeS_4. Adapted from Ref. [49].

4. Mixed-anion and mixed-cation alloys

Since the band gaps of Cu_2ZnSnS_4 and $Cu_2ZnSnSe_4$ are 1.5 eV and 1.0 eV, respectively, there is a 0.5 eV space for the band gap tuning through forming the S-Se alloys. It is interesting to see that the solar cells based on the mixed-anion $Cu_2ZnSn(S,Se)_4$ (CZTSSe) alloys have higher efficiency than those based on the pure Cu_2ZnSnS_4 (CZTS) and $Cu_2ZnSnSe_4$ (CZTSe) compounds,[2,51] although CZTS has an optimal band gap for single-junction solar cells according to the Shockley–Queisser model.[52] The physical properties of various alloys based on CZTS have been studied by several groups,[53–56] which are very important for understanding the better performance of the CZTS-based alloys. In order to simulate the random occupation of S and Se on the anion sites of the CZTSSe alloys, we used the special quasi-random structure (SQS) method[50,57] to describe the geometrical structure of the CZTSSe alloys. To know the miscibility of the alloys, the alloy formation enthalpy is defined as

$$\Delta H = E(x) - (1-x)E_{\mathrm{CZTS}} - xE_{\mathrm{CZTSe}},$$

where E_{CZTS} and E_{CZTSe} are the total energy of pure CZTS and CZTSe in the kesterite structure (the structure of the alloys is based on the kesterite structure unless otherwise specified), and $E(x)$ is the total energy of the alloy $Cu_2ZnSn(S_{1-x}Se_x)_4$.

At the same time, for most alloys, the alloy formation enthalpy obeys a quadratic function of the composition x

$$\Delta H = (1-x)\Delta H(0) + x\Delta H(1) + \Omega x(1-x),$$

where Ω is the interaction parameter that describes the alloy solubility.

The bandgap dependence of the conventional semiconductor alloys on the composition x follows the function

$$E_g(x) = (1-x)E_g(\mathrm{CZTS}) + xE_g(\mathrm{CZTSe}) - bx(1-x),$$

where b is the bowing parameter and E_g is the bandgap.

From Fig. 8, the interaction parameter Ω of CZTSSe is 26 meV/atom by fitting the enthalpy of composition x, which is much smaller than that of $Cu(In_xGa_{1-x})Se_2$ (CIGS) alloys,[58] so the problem of phase separation and inhomogeneity of CZTSSe can be avoided. The miscibility temperature of the CZTSSe alloy was predicted to be lower than 300 K

by applying the mean-field theory to the free energy of the solid solution, indicating that the CZTSSe alloy is stable at the room temperature.

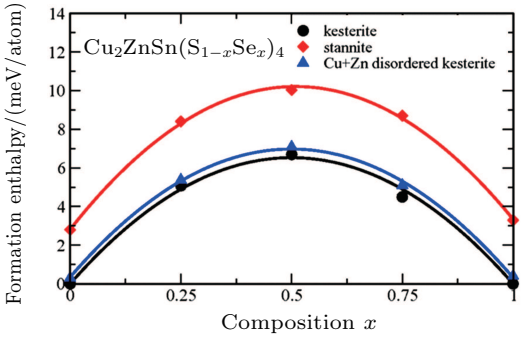


Fig. 8. (color online) The calculated enthalpy of formation for $Cu_2ZnSn(S_{1-x}Se_x)_4$ alloys as a function of composition x. Adapted from Ref. [42].

In Fig. 9, the bowing parameter of CZTSSe is 0.10 eV, which is close to that of $CuIn(S_{1-x}Se_x)_2$ (0.04 eV)[58] and $CuGa(S_{1-x}Se_x)_2$ (0.07 eV) alloys.[9] The bandgap of the CZTSSe alloys is nearly a linear function of the composition x, and the value decreases as x increases from 0 to 1, with the CBM level shifting down by 0.35 eV while the VBM level shifting up by 0.15 eV. According to the doping limit rule,[59] the CZTSSe alloys with high Se concentration can be more easily type-inverted to n-type because of the lower CBM as shown in Fig. 5(b). The easier type-inversion may be one reason for why the solar cells based on the CZTSSe alloys with high Se composition have a higher efficiency.[42,60]

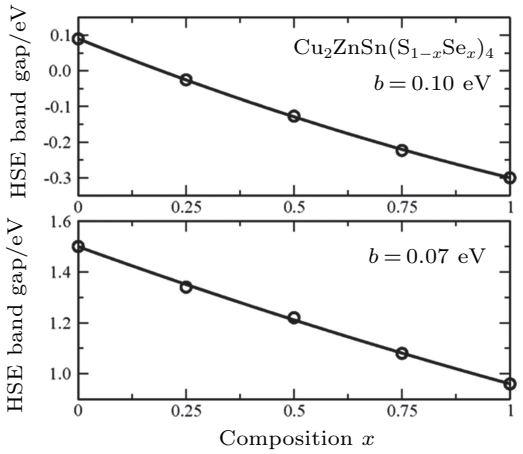


Fig. 9. (color online) The calculated bandgaps of the $Cu_2ZnSn(S_{1-x}Se_x)_4$ alloys using the (a) GGA functional and (b) HSE functional, respectively. Adapted from Ref. [42].

Besides the mix-anion alloys, several theoretical groups also studied the mixed-cation alloys, including $(Cu,Li)_2ZnSnS_4$,[61] $Cu_2(Zn,Fe)SnS_4$(CZFSS),[62] $Cu_2(Zn,Cd)SnS_4$,[63] $Cu_2Zn(Sn,Si)S_4$,[64] $Cu_2Zn(Sn,Ge)Se_4$,[64] and $(Cu,Ag)_2ZnSn(S,Se)_4$.[60] Shu *et al.* studied the properties of the $Cu_2Zn(Sn,Si)S_4$ and $Cu_2Zn(Sn,Ge)S_4$ alloys.[64] They found that the $Cu_2ZnSn_{1-x}Ge_xSe_4$ alloys are highly miscible and their band gap increases from 1.0 eV to 1.5 eV with composition x increasing from 0 to 1, while the $Cu_2ZnSn_{1-x}Si_xSe_4$ alloys are much less miscible and span a bandgap range from 1.0 eV to 2.4 eV. The bowing parameter of the $Cu_2Zn(Sn,Ge)S_4$ alloy is much smaller than that of $Cu_2Zn(Sn,Si)S_4$, because the size and chemical differences between Sn and Si are larger. Shen *et al.* investigated the electronic and optical properties of $Cu_2ZnGe(Se_xS_{1-x})_4$ alloy and found that the gap size may range from 1.52 eV to 2.25 eV, which will provide potential applications as solid state lighting[65] and water splitting photocatalyst. Shibuya *et al.* found that Fe can be easily mixed into CZTS.[62] It is interesting to see that the structure of $Cu_2Zn_{1-x}Fe_xSnS_4$ alloys changes from kesterite to stannite at $x = 0.4$, which may result in a small discontinuity of the bandgap. The CZFTS alloys with high Fe concentrations may be used in the Si-based tandem solar cells. Other groups[61,63] tuned the bandgap from 1.55 eV to 1.09 eV through $Cu_2(Zn,Cd)SnS_4$, and from 1.5 eV to 1.9 eV through $(Cu,Li)_2ZnSnS_4$. These alloys are also good candidates for tandem solar cells.

Not only the component-uniform mixed-anion and mixed-cation alloys, but also the component-graded $(Cu,Ag)_2ZnSn(S,Se)_4$ have been proposed to improve the photovoltaic performance of kesterite solar cells. The efficiency increase of kesterite solar cells stopped after the latest record efficiency was reported in 2013, and it is believed that there is a bottleneck to the further improvement of the open-circuit voltage (V_{oc}) and thus the efficiency. Yuan *et al.* proposed that one key origin of this bottleneck is that the Cu_{Zn} antisite defects can form very easily in Cu_2ZnSnS_4 (also in $Cu_2ZnSnSe_4$), making the material always p-type and cannot be doped easily to n-type under equilibrium condition, which pins the Fermi energy at the p–n junction and thus limits the V_{oc}.[60] They found that the easy formation of the antistie acceptor defects results from the high valence band (Cu 3d states) of the Cu_2ZnSnS_4, rather than the previously believed small size difference. However, their formation can be largely suppressed through replacing Cu by Ag (group I) to form Ag_2ZnSnS_4, which has a much lower valence band (due to the low Ag 4d states). This defect disparity opens up a possibility to overcome the V_{oc} limit of the Cu_2ZnSnS_4 and $Cu_2ZnSnSe_4$ solar cells. However, several high-concentration donor defects in Ag_2ZnSnS_4 and $Ag_2ZnSnSe_4$ have deep levels in the band gap and are thus possible recombination centers, so the efficiency of solar cells based on the pure Ag_2ZnSnS_4 and $Ag_2ZnSnSe_4$ will still be limited.[60]

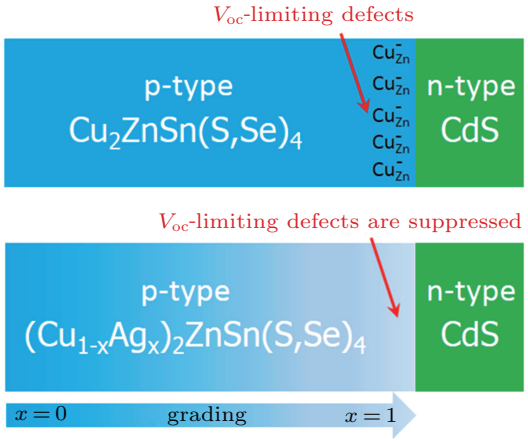


Fig. 10. (color online) Schematic plot of the p–n junction interface between the n-type CdS buffer layer and p-type absorber layer: $Cu_2ZnSn(S,Se)_4$ with high concentration of Cu_{Zn} antisite defects limiting V_{oc} (top) and component-graded $(Cu_{1-x}Ag_x)_2ZnSn(S,Se)_4$ alloys free of V_{oc}-limiting Cu_{Zn} defects (bottom). Adapted from Ref. [60].

To combine the advantages of Ag_2ZnSnS_4 and Cu_2ZnSnS_4, they proposed that the component-graded $(Cu,Ag)_2ZnSnS_4$ and $(Cu,Ag)_2ZnSnSe_4$ alloys can be ideal absorber layer materials if the Ag component is low in the interior of the absorber layer (thus less recombination-center defects) but high near the p–n junction interface (thus less V_{oc}-limiting defects).[60] The component-graded $(Cu,Ag)_2ZnSnSe_4$ absorber layers have great potential to increase the V_{oc} and thus improve the solar cell efficiency. This strategy for overcoming the V_{oc} limit has be demonstrated recently by the interesting experimental work of Guchhait *et al.* who developed a new solution processable method for the Ag incorporation and observed an increase in open-circuit voltage V_{oc} by 50 mV and an accompanying rise in device efficiency from 4.9% to 7.2%.[66] More recently, Qi *et al.* demonstrated a significant increase in V_{oc} by appropriately adjusting the Ag gradient in a double-graded $(Cu,Ag)_2ZnSn(S,Se)_4$ alloy, and an unexpected conversion efficiency of 11.2%, which is the highest efficiency achieved to date for the component-graded $(Cu,Ag)_2ZnSn(S,Se)_4$ alloy solar cells,[67] supporting a new aspect that synthesis of a component-graded $(Cu,Ag)_2ZnSn(S,Se)_4$ absorber has great potential for future research.[67]

5. Alkali dopants

The beneficial effect of alkali-metal dopants on $Cu(In,Ga)Se_2$ thin film solar cells has been investigated for several decades. The alkali-metal can be doped into the lattice of $Cu(In,Ga)Se_2$, compensating the donors or promoting the acceptor carrier concentration in the absorber layer,[68–71] and can also increase the grain size and passivate the grain boundaries (GB) which act as the recombination centers in the thin films.[68]

Inspired by the prominent effect of alkali-doped $Cu(In,Ga)Se_2$ devices, it is expected that the alkali metals will also have beneficial effects on CZTS and CZTSe based solar cells because of the similar crystal and device structures. Using the first-principles calculations, Maeda *et al.* studied the doping effect of Li, Na, and K in CZTS and CZTSe.[72] Their results show that alkali metal is prone to occupy the Zn site first, then the Cu site, followed by the Sn site and the interstitial site. The substitution defect of alkali metal on the Zn site will be the primary p-type defect in CZTS and CZTSe. However, in the study of Xiao *et al.*,[73] Na_{Cu} has the lowest formation energy, but Na_{Cu} is an isovalent substitution which cannot produce carriers and increase the hole concentration. Whereas, the formation energy of Na_{Zn} is a little higher than that of Na_{Cu}, which will contribute to the electrical conductivity of the CZTS absorber layer. The difference of the two studies results from the different chemical potentials considered in their calculations. In 2016, Yuan *et al.* proposed a new picture on why the isovalent Na_{Cu} substitution can increase the hole carrier concentration based on the Na diffusion in the lattice,[70] which opens a new view on the role of sodium in promoting the hole concentration from the electronic point of view.

Meanwhile, calculations on the transition energy levels of Na dopants on different sites revealed that Na_{Zn} is a shallow acceptor. Although Na_{Sn} introduces two transition energy levels, one of which is close to the middle of the band gap, the formation energy of Na_{Sn} is so high that its detrimental effect as recombination center can be ignored.

Experimentally, Heish *et al.* investigated the efficiency enhancement via alkali metal doping on CZTSSe. They found that small alkali metals are suitable for increasing the carrier concentration because they are easy to substitute the lattice atom in CZTSSe, while the larger alkali metals are favorable for increasing the grain size because of the low melting point of binary selenides, which will suppress the non-radiative recombination caused by the GBs, since less GBs are produced in the absorber layer.[74]

The benign effect of alkali metal on the increase of the carrier concentration in CZTSSe has also been proved by several previous studies,[75–77] where one order of increment of the carrier concentration was obtained by doping sodium into CZTS.[75] It seems that the alkali metal has the similarly beneficial effect as that in CIS. The enhancement of the mobility of the hole carriers was also observed by Nagaoka *et al.*[77] Moreover, Zhao *et al.* calculated the effective mass of holes in the CZTS with Na impurity, and found that effective mass of hole in Na-doped CZTS is lighter, implying that Na benefits the hole mobility in CZTS.

Based on the observation of Prabhakar *et al.*,[75] Na impurity in CZTS enhances the (112) texture of the film.

Also, potassium was shown to enhance the (112) preferred orientation,[78] which indicates that the alkali metal improves the crystallinity of the film. The improvement of the grain size was also observed after introducing Li,[74,79] Na,[74,75,77,79,80] K,[74,80] Rb,[74,79] and Cs.[74] It is worth noting that the grain size reaches its maximum at 1% K doping and decreases as the K doping concentration continues rising as reported in the study of Tong *et al.*[78] Based on the aforementioned studies, the effect of the alkali metal on the grain size cannot be drew out, but a detailed investigation of the sodium concentration in CZTS grains has pointed out that the electronic passivation of the GB requires less sodium than that required for producing large grains.[81] This means that the size of the grain becomes not critical to the solar cell performance as long as the GB is electronically passivated.

Based on the discussions above, it is clear that alkali metal also plays a beneficial role in CZTS, but it is still not clear whether the influence mechanism in CZTS is similar to that in Cu(In,Ga)Se_2. Further investigation on the effect of alkali metal in CZTS and CZTSe is necessary.

6. Grain boundaries

Besides the point defects, the grain boundaries of the CZTS and CZTSe thin films are also important for their photovoltaic performance. Usually the polycrystalline semiconductors exhibit a poorer performance in comparison with their monocrystalline counterparts, because there are usually dangling bonds, wrong bonds, and wrong bonding angles on the grain boundaries, which may introduce deep levels in the band gap and act as non-radiative recombination centers in the system.

The lack of experimental observations on the structures of grain boundaries in CZTS caused the difficulty in obtaining the exact atomic structure of the grain boundaries, however, the theoretical model of the grain boundaries in CZTS can be adopted from those in CdTe which had been observed via the high-resolution transmission electron microscopy (HRTEM).[82] Considering the ordered substitution of Cu, Zn, and Sn for the cation ions, CZTS has 4 different grain boundaries as shown in Fig. 11, where the GB-I type and GB-III type are anion-core prototype GB structures, and the GB-II type and GB-IV type are cation-core prototype GB structures. As some atoms on these boundaries are not tetrahedrally coordinated, some wrong bonds and dangling bonds are produced, which are the typical feature of polycrystalline semiconductors.

Several groups have investigated the feature of these GBs in CZTS. Li *et al.* calculated the density of states of the GB structures in Fig. 11,[83] showing that the wrong bonded atoms on the boundaries of CZTS will introduce deep levels in the bandgap of the bulk crystal. Although structural relaxation will remove these deep levels to a certain extent, it is still not as effective as those in CIS. Yin *et al.* calculated the band structure and the density of states of the CZTSe Σ3 (114) GB (the GB-III in Fig. 11) and concluded that the wrong bonds at GB will introduce deep levels, which will cause the Shockley–Read–Hall (SRH) recombination centers in the band gap and be detrimental to V_{oc} and J_{sc} in CZTS.[84] This is different from the case of CIS whose structure is also derived from that of CdTe, i.e., the grain boundary of CIS presents some intrinsic beneficial effects, such as creating a hole barrier and promoting the hole-electron separation, large relaxation in GB moves the defect states into the valence band.[85,86] These effects made polycrystalline CIS exhibit better performance in comparison with its crystalline counterparts, however, this feature is not inherited by CZTS.

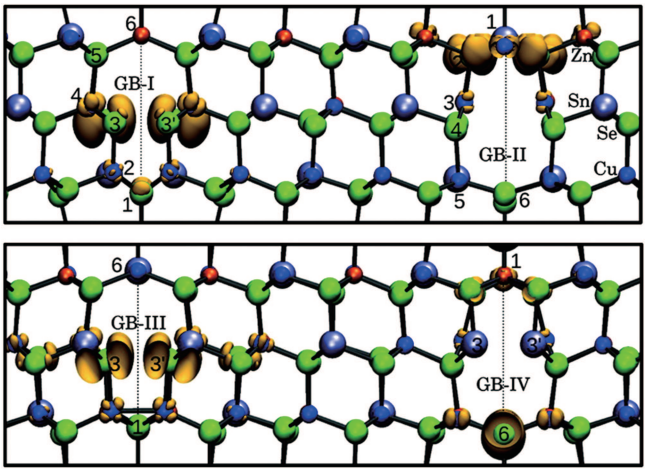


Fig. 11. (color online) The 4 relaxed atomic structures of $Cu_2ZnSnSe_4$ GBs. The grain boundary (114) plane is indicated by the dashed line. Adapted from Ref. [83].

Experimentally, Kim *et al.* found that the highest efficiency samples of CZTS exhibit downward potential bending at GB area and upward bending at the inter-grains, while the poorer efficiency samples exhibit an opposite behavior,[87] which shows that the quality of the GB strongly affects the property of the CZTS devices.

Since the intrinsic GB of CZTS is detrimental, an important issue of the GB in CZTS is whether it can be passivated or not. Using DFT calculation, Yin *et al.* found the segregation of Zn_{Sn}, O_{Se}, and Na_i has the beneficial effect of eliminating the deep defect states in the band gap and creating a hole barrier at GB.[84] Liu *et al.* found that Na not only can passivate the deep level in the band gap, but also prefers to segregate at the GBs of CZTS because it has negative formation energies in the system.[88] These calculation studies pointed out the potential passivation method that can be applied on CZTS to ensure the improvement of GB in CZTS.

The effect of sodium in the GB of CZTS was studied by Gerson experimentally, who demonstrated that the CZTS samples without sodium treatment contain non-radiative recombination center defects, and these deep-level defects can be effectively passivated by the addition of sodium.[81] Sodium prefers to locate on the surface and GBs of CZTS and it can help to produce large grains, and a small amount of sodium is sufficient to passivate GBs effectively.

7. Conclusions and remarks

The number of component elements increased steadily in the 60-year development of photovoltaic semiconductors, i.e., from silicon in 1950s, to GaAs and CdTe in 1960s, $CuInSe_2$ in 1970s, $Cu(In,Ga)Se_2$ in 1980s, Cu_2ZnSnS_4 in 1990s, and more recently $Cu_2ZnSn(S,Se)_4$ and $CH_3NH_3PbI_3$. The increased number of elements in Cu_2ZnSnS_4 and $Cu_2ZnSnSe_4$ and their alloys $Cu_2ZnSn(S,Se)_4$ relative to binary II–VI or III–V semiconductors results in the increased structural and chemical freedom for tuning the material properties. We reviewed how these group I_2–II–IV–VI_4 semiconductors can be derived from the binary II–VI semiconductors through element-mutation, i.e., from II–VI (ZnS) to I–III–VI_2 ($CuGaS_2$) and then to I_2–II–IV–VI_4 (Cu_2ZnSnS_4). Following the mutation, we can determine the crystal structures of the I_2–II–IV–VI_4 semiconductors and reveal the chemical trends in their electronic band structure, which makes the band structure engineering possible. The band gaps of I_2–II–IV–VI_4 compounds can be tuned from negative (metal or topological insulator[89]) to more than 4 eV (wide-gap semiconductor). Furthermore, the increased structural freedom enhances the miscibility (component-uniformity) of the $Cu_2ZnSn(S,Se)_4$ and $Cu_2Zn(Sn,Ge)Se_4$ alloys, so their band gaps can be tuned continuously and also linearly as a function of the alloy composition.

The easy formation of Cu_{Zn} antisite defect and related defect complexes was believed to be one critical factor limiting the open-circuit voltage and efficiency of kesterite solar cells. In order to suppress the formation of these defects, the mixed-cation $(Ag,Cu)_2ZnSn(S,Se)_4$ and $Cu_2(Zn,Cd)Sn(S,Se)_4$ alloys were proposed as alternative light-absorber layers and are now under intensive study. The recent experimental breakthrough on the component-graded $(Ag,Cu)_2ZnSn(S,Se)_4$ alloy solar cells may point out a possible direction or method for breaking the 12.6% efficiency record.

The increased structural and chemical freedom also causes the dramatic increase of possible point defects in the lattice of $Cu_2ZnSn(S,Se)_4$ thin films, which can significantly influence the optical and electrical properties and thus the photovoltaic performance. A series of point defects have been predicted since 2010.[24,90–92] After that various defect levels have been experimentally observed using different characterization techniques, and compared with the calculated defect levels. Although the ionization levels of the dominant defects such as Cu_{Zn} and V_{Cu} have been experimentally well confirmed, other defect levels have not well determined. A careful and systematical characterization of the defect levels in Cu_2ZnSnS_4 and $Cu_2ZnSnSe_4$ and their alloys $Cu_2ZnSn(S,Se)_4$ with different chemical composition ratios and different growth techniques will be very useful for the knowledge-based defect optimization. Although the defect properties are not reviewed here, the importance of the defect optimization cannot be neglected.

Besides the intrinsic defects, extrinsic elements may be doped into these quaternary semiconductors intentionally or unintentionally. Whether the real thin films can work as ideal light-absorber layers depends also on the behavior of the possible extrinsic dopants. Here we reviewed the study on the alkaline dopants which may exist in both the grain interiors and on the grain boundaries. Many opinions that were proposed for understanding the alkaline dopants and grain boundaries in $Cu(In,Ga)Se_2$ solar cells have been borrowed in the study of the alkaline dopants and grain boundaries in Cu_2ZnSnS_4, $Cu_2ZnSnSe_4$, and $Cu_2ZnSn(S,Se)_4$. However, obvious differences in these properties have been found between $Cu(In,Ga)Se_2$ and $Cu_2ZnSn(S,Se)_4$. More careful, accurate, and systematical studies on the alkaline dopants and grain boundaries in the kesterite solar cells are still necessary and fundamental to the search for new strategies for the performance optimization.

The interfaces between the kesterite Cu_2ZnSnS_4, $Cu_2ZnSnSe_4$, and $Cu_2ZnSn(S,Se)_4$ and CdS are currently not well-studied, because the microstructure near the interfaces can be very complicated and also depend on the specific fabrication methods and conditions. It is not clear whether the interfaces between the kesterite absorber layer and CdS are similar to those between the chalcopyrite absorber layer and CdS, so it is still an open question whether the kesterite solar cells should inherit the device structure from the chalcopyrite thin film solar cells. Systematical simulation and characterization of these interfaces are of fundamental importance to the future development of high-efficiency kesterite solar cells.

References

[1] Chen S, Gong X, Walsh A and Wei S H 2009 *Appl. Phys. Lett.* **94** 041903
[2] Todorov T K, Reuter K B and Mitzi D B 2010 *Adv. Mater.* **22** E156
[3] Katagiri H, Jimbo K, Maw W S, Oishi K, Yamazaki M, Araki H and Takeuchi A 2009 *Thin Solid Films* **517** 2455
[4] Chen S 2016 *Semiconductor Materials for Solar Photovoltaic Cells* (Switzerland: Springer International Publishing) pp. 75–103
[5] Hahn H and Schulze H 1965 *Naturwiss* **52** 426
[6] Schleich D M and Wold A 1977 *Mater. Res. Bull.* **12** 111
[7] Parasyuk O V, Gulay L D, Romanyuk Y E and Piskach L V 2001 *J. Alloys Compd.* **329** 202
[8] Parasyuk O V, Piskach L V, Romanyuk Y E, Olekseyuk I D, Zaremba V I and Pekhnyo V I 2005 *J. Alloys Compd.* **397** 85

[9] Chen S, Gong X G, Walsh A and Wei S H 2009 *Phys. Rev. B* **79** 165211
[10] Chen S, Walsh A, Luo Y, Yang J H, Gong X G and Wei S H 2010 *Phys. Rev. B* **82** 195203
[11] Cai Z H, Narang P, Atwater H A, Chen S Y, Duan C G, Zhu Z Q and Chu J H 2015 *Chem. Mater.* **27** 7757
[12] Fan F J, Wu L and Yu S H 2014 *Energy Environ. Sci.* **7** 190
[13] Walsh A, Chen S, Wei S H and Gong X G 2012 *Adv. Energy Mater.* **2** 400
[14] Chen S, Narang P, Atwater H A and Wang L W 2014 *Adv. Mater.* **26** 311
[15] Narang P, Chen S, Coronel N C, Gul S, Yano J, Wang L W, Lewis N S and Atwater H A 2014 *Adv. Mater.* **26** 1235
[16] Ito K and Nakazawa T 1988 *Jpn. J. Appl. Phys.* **27** 2094
[17] Katagiri H 1996 *Tech. Dig. 9th International Photovoltaic Science and Engineering Conference,* Miyazaki, p. 745
[18] Friedlmeier T M, Wieser N, Walter T, Dittrich H and Schock H W 1997 *Proceedings of the 14th European Photovoltaic Solar Energy Conference*, Barcelona, Spain, p. 1242
[19] Madelung O 2004 *Semiconductors: Data Handbook* (New York: Springer)
[20] Schorr S 2011 *Sol. Energy Mater. Sol. Cells* **95** 1482
[21] Todorov T K, Tang J, Bag S, Gunawan O, Gokmen T, Zhu Y and Mitzi D B 2013 *Adv. Energy Mater.* **3** 34
[22] Wang W, Winkler M T, Gunawan O, Gokmen T, Todorov T K, Zhu Y and Mitzi D B 2013 *Adv. Energy Mater.* **4** 1301465
[23] Ahn S, Jung S, Gwak J, Cho A, Shin K, Yoon K, Park D, Cheong H and Yun J H 2010 *Appl. Phys. Lett.* **97** 021905
[24] Chen S, Walsh A, Gong X G and Wei S H 2013 *Adv. Mater.* **25** 1522
[25] Yuan Z K, Xu P and Chen S Y 2015 *Acta Phys. Sin.* **64** 186102 (in Chinese)
[26] Bernard J E, Ferreira L G, Wei S H and Zunger A 1988 *Phys. Rev. B* **38** 6338
[27] Magri R, Wei S H and Zunger A 1990 *Phys. Rev. B* **42** 11388
[28] Zhang Y, Sun X, Zhang P, Yuan X, Huang F and Zhang W 2012 *J. Appl. Phys.* **111** 063709
[29] Satoshi N, Tsuyoshi M and Takahiro W 2010 *Jpn. J. Appl. Phys.* **49** 121203
[30] Schorr S, Hoebler H J and Tovar M 2007 *Eur. J. Mineral.* **19** 65
[31] Washio T, Nozaki H, Fukano T, Motohiro T, Jimbo K and Katagiri H 2011 *J. Appl. Phys.* **110** 074511
[32] Wang C C, Chen S Y, Yang J H, Lang L, Xiang H J, Gong X G, Walsh A and Wei S H 2014 *Chem. Mater.* **26** 3411
[33] Zhong G, Tse K, Zhang Y, Li X, Huang L, Yang C, Zhu J, Zeng Z, Zhang Z and Xiao X 2016 *Thin Solid Films* **603** 224
[34] Liu C Y, Zhang Y Y, Hou Y S, Chen S Y, Xiang H J and Gong X G 2016 *Phys. Rev. B* **93** 205426
[35] Xiao Z, Meng W, Li J V and Yan Y 2017 *ACS Energy Lett.* **2** 29
[36] Chen R and Persson C 2017 *J. Appl. Phys.* **121** 203104
[37] Chen S Y, Gong X G, Walsh A and Wei S H 2011 *Physics* **40** 248 (in Chinese)
[38] Zhang L J, Zhang B P, Ge Z H, Han C G, Chen N and Li J F 2013 *Intermetallics* **36** 96
[39] Paier J, Asahi R, Nagoya A and Kresse G 2009 *Phys. Rev. B* **79** 115126
[40] Nakamura S, Maeda T and Wada T 2009 *Phys. Status Solidi* **6** 1261
[41] Zou D, Nie G, Li Y, Xu Y, Lin J, Zheng H and Li J 2015 *RSC Adv.* **5** 24908
[42] Chen S, Walsh A, Yang J H, Gong X G, Sun L, Yang P X, Chu J H and Wei S H 2011 *Phys. Rev. B* **83** 125201
[43] Palsgaard M L N, Crovetto A, Gunst T, Markussen T, Hansen O, Stokbro K and Brandbyge M 2016 2016 *International Conference on Simulation of Semiconductor Processes and Devices (SISPAD)*, pp. 377–380
[44] Nagoya A, Asahi R and Kresse G 2011 *J. Phys.: Condens. Matter* **23** 404203
[45] Dong Z Y, Li Y F, Yao B, Ding Z H, Yang G, Deng R, Fang X, Wei Z P and Liu L 2014 *J. Phys. D: Appl. Phys.* **47** 075304
[46] Bao W and Ichimura M 2012 *Int. J. Photoenergy* **2012** 619812
[47] Bao W and Ichimura M 2012 *Jpn. J. Appl. Phys.* **51** 10NC31
[48] Yu J L, Zheng Z M, Dong L M, Cheng S Y, Lai Y F, Zheng Q, Zhou H F, Jia H J, Zhang H 2017 *Chin. Phys. B* **26** 046802
[49] Liu H R, Chen S, Zhai Y T, Xiang H J, Gong X G and Wei S H 2012 *J. Appl. Phys.* **112** 093717
[50] Chen S, Gong X G and Wei S H 2007 *Phys. Rev. B* **75** 205209
[51] Guo Q, Ford G M, Yang W C, Walker B C, Stach E A, Hillhouse H W and Agrawal R 2010 *J. Am. Chem. Soc.* **132** 17384
[52] Shockley W and Queisser H J 1961 *J. Appl. Phys.* **32** 510
[53] Dun C, Holzwarth N a W, Li Y, Huang W and Carroll D L 2014 *J. Appl. Phys.* **115** 193513
[54] Dimitrievska M, Xie H, Fairbrother A, Fontané X, Gurieva G, Saucedo E, Pérez-Rodríguez A, Schorr S and Izquierdo-Roca V 2014 *Appl. Phys. Lett.* **105** 031913
[55] Khare A, Himmetoglu B, Cococcioni M and Aydil E S 2012 *J. Appl. Phys.* **111** 123704
[56] Zamulko S, Chen R and Persson C 2017 *Phys. Status Solidi* **254** 1700084
[57] Wei S H, Ferreira L G, Bernard J E and Zunger A 1990 *Phys. Rev. B* **42** 9622
[58] Wei S H and Zunger A 1995 *J. Appl. Phys.* **78** 3846
[59] Zhang S B, Wei S H and Zunger A 1998 *J. Appl. Phys.* **83** 3192
[60] Yuan Z K, Chen S, Xiang H, Gong X G, Walsh A, Park J S, Repins I and Wei S H 2015 *Adv. Funct. Mater.* **25** 6733
[61] Lafond A, Guillot-Deudon C, Vidal J, Paris M, La C and Jobic S 2017 *Inorg. Chem.* **56** 2712
[62] Shibuya T, Goto Y, Kamihara Y, Matoba M, Yasuoka K, Burton L A and Walsh A 2014 *Appl. Phys. Lett.* **104** 021912
[63] Xiao Z Y, Li Y F, Yao B, Deng R, Ding Z H, Wu T, Yang G, Li C R, Dong Z Y, Liu L, Zhang L G and Zhao H F 2013 *J. Appl. Phys.* **114** 183506
[64] Shu Q, Yang J H, Chen S, Huang B, Xiang H, Gong X G and Wei S H 2013 *Phys. Rev. B* **87** 115208
[65] Shen K, Jia G, Zhang X and Jiao Z 2016 *Mol. Phys.* **114** 2948
[66] Guchhait A, Su Z, Tay Y F, Shukla S, Li W, Leow S W, Tan J M R, Lie S, Gunawan O and Wong L H 2016 *ACS Energy Lett.* **1** 1256
[67] Qi Y F, Kou D X, Zhou W H, Zhou Z J, Tian Q W, Meng Y N, Liu X S, Du Z L and Wu S X 2017 *Energy Environ. Sci.* **10** 2401
[68] Contreras M A, Egaas B, Dippo P, Webb J, Granata J, Ramanathan K, Asher S, Swartzlander A and Noufi R 1997 26*th IEEE Photovoltaic Specialists Conference, IEEE Anaheim*, California, USA, pp. 359–362
[69] Wei S H, Zhang S and Zunger A 1999 *J. Appl. Phys.* **85** 7214
[70] Yuan Z K, Chen S, Xie Y, Park J S, Xiang H, Gong X G and Wei S H 2016 *Adv. Energy Mater.* **6** 1601191
[71] Niles D W, Al-Jassim M and Ramanathan K 1999 *J. Vac. Sci. Technol. A* **17** 291
[72] Maeda T, Kawabata A and Wada T 2015 *Phys. Status Solidi C* **12** 631
[73] Xiao W, Wang J, Zhao X, Wang J, Huang G, Cheng L, Jiang L and Wang L 2015 *Sol. Energy* **116** 125
[74] Hsieh Y T, Han Q, Jiang C, Song T B, Chen H, Meng L, Zhou H and Yang Y 2016 *Adv. Energy Mater.* **6** 1502386
[75] Prabhakar T and Jampana N 2011 *Sol. Energy Mater. Sol. Cells* **95** 1001
[76] Zhou H, Song T B, Hsu W C, Luo S, Ye S, Duan H S, Hsu C J, Yang W and Yang Y 2013 *J. Am. Chem. Soc.* **135** 15998
[77] Nagaoka A, Miyake H, Taniyama T, Kakimoto K, Nose Y, Scarpulla M A and Yoshino K 2014 *Appl. Phys. Lett.* **104** 152101
[78] Tong Z, Yan C, Su Z, Zeng F, Yang J, Li Y, Jiang L, Lai Y and Liu F 2014 *Appl. Phys. Lett.* **105** 223903
[79] Altamura G, Wang M and Choy K L 2016 *Sci. Rep.* **6** 22109
[80] Johnson M, Baryshev S, Thimsen E, Manno M, Zhang X, Veryovkin I, Leighton C and Aydil E 2014 *Energy Environ. Sci.* **7** 1931
[81] Gershon T, Shin B, Bojarczuk N, Hopstaken M, Mitzi D B and Guha S 2015 *Adv. Energy Mater.* **5** 1400849
[82] Yan Y, Al-Jassim M and Jones K 2003 *J. Appl. Phys.* **94** 2976
[83] Li J, Mitzi D B and Shenoy V B 2011 *ACS Nano* **5** 8613
[84] Yin W J, Wu Y, Wei S H, Noufi R, Al-Jassim M M and Yan Y 2014 *Adv. Energy Mater.* **4** 1
[85] Yan Y, Noufi R and Al-Jassim M 2006 *Phys. Rev. Lett.* **96** 205501
[86] Persson C and Zunger A 2003 *Phys. Rev. Lett.* **91** 266401
[87] Kim G Y, Jeong A R, Kim J R, Jo W, Son D H, Kim D H and Kang J K 2014 *Sol. Energy Mater. Sol. Cells* **127** 129
[88] Liu C Y, Li Z M, Gu H Y, Chen S Y, Xiang H and Gong X G 2016 *Adv. Energy Mater.* **7** 1601457
[89] Chen S, Gong X G, Duan C G, Zhu Z Q, Chu J H, Walsh A, Yao Y G, Ma J and Wei S H 2011 *Phys. Rev. B* **83** 245202
[90] Chen S, Gong X, Walsh A and Wei S H 2010 *Appl. Phys. Lett.* **96** 021902
[91] Chen S, Yang J H, Gong X, Walsh A and Wei S H 2010 *Phys. Rev. B* **81** 245204
[92] Chen S, Wang L W, Walsh A, Gong X G and Wei S H 2012 *Appl. Phys. Lett.* **101** 223901